ELSEVIER

Journal of Magnetism and Magnetic Materials 231 (2001) 315–322

Journal of magnetism and magnetic materials

www.elsevier.com/locate/jmmm

X-ray absorption spectra and X-ray magnetic circular dichroism studies at Fe and Co $L_{2,3}$ edges of mixed cobalt–zinc ferrite nanoparticles: cationic repartition, magnetic structure and hysteresis cycles

J.F. Hochepied[a,b], Ph. Sainctavit[c,d], M.P. Pileni[b,*]

[a] *C.E.A.- C.E. Saclay, DRECAM-S.C.M, 91191 Gif sur Yvette Cedex, France*

[b] *Laboratoire LM2N, ESA 1070, Universite Pierre et Marie Curie, (Paris VI), BP 52, 4 Place Jussieu, 75231 Paris Cedex 05, France*

[c] *Laboratoire de Minéralogie et Cristallographie, UMR CNRS 7590, UPMC/UDD/IPGP, case115, 4 place Jussieu, 75252 Paris Cedex 05, France*

[d] *Laboratoire pour l'Utilisation du Rayonnement Electromagnétique (LURE), UMR 130, Université Paris Sud, Bât 109d, 91405 Orsay Cedex, France*

Received 4 October 2000; received in revised form 14 February 2001

Abstract

X-ray absorption spectra (XAS) and X-ray magnetic circular dichroism (XMCD) spectra at Co and Fe $L_{2,3}$ edges are performed on mixed cobalt–zinc ferrite nanoparticles $Co_{0.73y}Zn_{0.73(1-y)}Fe_{2.18}\square_{0.09}\ O_4$ (with $y=0.4$, 2.8 and 3.7 nm average diameter; the symbol $\square$ represents a vacancy). Simulation of the spectra thanks to ligand field multiplet theory allows an evaluation of the cationic repartition. Co^{2+} occupies preferentially octahedral sites for the studied composition, its magnetic moment is 3.64 μ_B, consistent with well-known bulk values for pure cobalt ferrite. Hysteresis curves are measured thanks to XMCD spectra and compared to magnetometry measurements. Being chemically selective, XMCD technique is found promising to complete magnetometry measurements on systems involving several magnetic ions. © 2001 Published by Elsevier Science B.V.

PACS: 61.46; 75.50.K; 75.50.G; 78.70.D; 78.20.L

Keywords: Ferrite; Nanoparticles; X-ray magnetic circular dichroism; Coercivity; Magnetic anisotropy

1. Introduction

Ferrite nanoparticles are a subject of interest as far as fundamental aspects of magnetism are concerned (superparamagnetism [1,2], spin-canting [3–8]) but also because of a large field of applications (information storage [9], ferrofluids, contrasting agents in medical imaging, magnetic carriers used in medecine [10]). Due to their various obtention methods, ferrite nanoparticles often exhibit a wide range behaviors as far as their magnetic properties are concerned. The main

*Corresponding author. Tel.: +33-1-44-27-25-16; fax: +33-1-44-27-25-15.

E-mail address: pileni@sri.fussi.eu.fr (M.P. Pileni).

0304-8853/01/$ - see front matter © 2001 Published by Elsevier Science B.V.
PII: S0304-8853(01)00182-2

complication results from the mixing of intrinsic size or surface effects with crystallinity and cationic distribution effects [11–13]. Hence for a good monitoring of specific properties of these nanoparticles it is absolutely necessary to have the deeper knowledge of their crystallographic, electronic and magnetic structures. Nanometric ferrites obtained by soft chemistry methods are generally well crystallized, although cationic distribution disorder might be important. Hence in ferrite nanoparticles chemical and magnetic disorder can be responsible for peculiar behavior (surface spin canting) that has no equivalent in bulk systems.

To study the magnetic and cationic structure of nanoferrites, a magnetic, chemically selective and site sensitive probe is required. Generally neutron diffraction is used, but it supposes well crystallized and rather large nanoparticles to allow good refinements, and if the compound contains many different ions (as mixed ferrites) the interpretation may become difficult or even impossible if atomic diffusion factors are too close.

A powerful investigation method, fulfilling these requirements, is the X-ray magnetic circular dichroism (XMCD) at the cation $L_{2,3}$ edges. Here we study XMCD of mixed cobalt–zinc ferrite nanoparticles at Fe and Co $L_{2,3}$ edges, in order to determine their magnetic structure and cationic distribution. The $L_{2,3}$ edges of Fe and Co correspond to transitions from the 2p bound states towards the 3d unoccupied levels. In XMCD measurements at the $L_{2,3}$ edges one then probes the levels that are responsible for the dielectric and magnetic properties. Elements are easily separated by the values of their edges and XMCD is sensitive to the site symmetry of the absorbing ion and to the orientation and amplitude of the local magnetic moments. Through the theoretical analysis of the XMCD signals, one can also separates the orbital and spin contributions to the total magnetic moments.

The following studies have several goals: the determination of Co^{2+} location in the structure, since Co^{2+} ions are responsible for the high magnetocrystalline anisotropy of cobalt ferrite but only if they occupy octahedral sites; the comparison between information obtained from isotropic XAS and XMCD results, leading to a description of the magnetic structure of diluted ferrite (nonstoichiometric zinc ferrite); and finally the measurement of element-specific hysteresis cycles.

2. Experimental section

Ferrite nanoparticles of formula $Co_{0.73y}Zn_{0.73(1-y)}Fe_{2.18}\square_{0.09}O_4$ are obtained by direct micelles syntheses [14] performed at 30°C. Various relative amounts of divalent dodecylsulfate, $X(DS)_2$, are solubilized in 10 ml aqueous solution. The iron dodecylsulfate concentration, $[Fe(DS)_2]$, and the relative percentage $[Fe(DS)_2]/\Sigma([X(DS)_2]$ are $C = 1.68 \times 10^{-2}$ M (samples A) or $C/2$ (samples B), and 0.75 respectively. The relative concentration of cobalt compared to zinc dodecylsulfate, $y = [Co(DS)_2]/([Co(DS)_2] + [Zn(DS)_2])$, varies from 0 to 1. After metylamine addition, solutions are stirred during 2 h then precipitated with ethanol and centrifugated. Precipitates are then washed several times with ethanol. The studied samples are characterized by a lognormal size distribution, measured after counting about 350 particles in transmission electron microscopy patterns

$$P(D) = \frac{1}{D\sigma\sqrt{2\pi}} \exp\left(-\frac{\ln^2(D/D_0)}{2\sigma^2}\right)$$

with parameters $D_0 = 3.7$ nm and $\sigma = 0.26$ for $y = 0$ (sample A0), $D_0 = 3.8$ nm and $\sigma = 0.23$ for $y = 0.40$ (sample A40), $D_0 = 2.8$ nm and $\sigma = 0.23$ for $y = 0.40$ (sample B40). The composition of the samples was verified by energy dispersive spectroscopy to be equal to the proportions used to perform syntheses [14]. From Mössbauer experiments [15] we assumed that no Fe^{2+} ions were in the structure, which explains the choice of a formula with vacancies (from composition, due to the spinel structure and the proportion of divalent Co^{2+} and Zn^{2+} ions, a maximum of only 10% of Fe cations could be in a +II oxidation state).

XAS spectra were performed at LURE on SUPER-ACO (line SU23). The white beam delivered by an asymmetric wiggler is monochromatized by a plane grating monochromator with

a high resolving power [16]. The figure of merit $E/\Delta E$ is estimated to be 3500. The polarization rate of the photons impinging on the sample is around 50%. The beam is perpendicular to the sample plane. The spectra were recorded in the total electron yield mode where the drain photocurrent, that is proportional to the absorption cross section, is measured. The sample is in ultra-high vacuum conditions (1×10^{-10} mbar). The sample temperature could be regulated between 300 and 3 K with a pumped ^{4}He cryostat and the magnetic field delivered by a superconducting coil could be varied from -4 T to $+4$ T. During the XMCD measurements, right and left circularly polarized photons are selected. Two spectra, $\sigma_{\uparrow\uparrow}$ and $\sigma_{\uparrow\downarrow}$, are registered with the magnetic field direction parallel or antiparallel to the propagation vector of the photons. In the electric dipole approximation reversing the magnetic field in an absorption measurement is equivalent to reversing the helicity of the photons. The XMCD signal is defined as the difference ($\sigma_{\uparrow\uparrow}-\sigma_{\uparrow\downarrow}$) between the two spectra.

Nanocrystals powders were dispersed in ethanol then dried on a copper grid. Measurements were performed from 770 to 820 eV for Co $L_{2,3}$ edges and from 700 eV to 750 eV for Fe $L_{2,3}$ edges. For all the measurements the energy step was 0.1 eV and the accumulation time was 1 s per point and the magnetic field was reversed at every scan. Each measurement plotted in this paper is the average of 3 scans for which a baseline was then substracted to allow comparison with calculations.

Calculations were performed in the Ligand Field Multiplet Theory [17]. This is an atomic model in which the electronic repulsions are considered through Slater integrals. These are calculated thanks to an atomic Hartree–Fock program and are scaled down by a reduction factor, κ, linked to the covalence degree of the chemical bonds: κ is the β coefficient of the nephelauxitic series. The atomic spin–orbit coupling parameters, ζ_{2p} and ζ_{3d}, are in a first time calculated through the monoelectronic potential around the ion, and then adjusted to improve the fit of the spectra. The surrounding of the ion is defined by an electrostatic potential with octahedral or tetrahedral symmetry. The strength of the crystal field potential is given by the parameter 10 Dq. In the Ligand Field Multiplet approach the radial integrals (Slater integrals, ζ_{2p} and ζ_{3d}, 10 Dq) are adjustable free parameters of the theory, that are partially constrained by the information gained from other spectroscopies. The intrinsic and instrumental resolutions are taken into account through Lorentzian and Gaussian broadening.

XAS spectra at Co $L_{2,3}$ edges for samples A40 and B40 (Fig. 1) are quite usual for octahedral Co^{2+} compounds [18]. Nevertheless comparison of the two samples exhibits a difference in the relative height of peaks B–C and D for L_3 edge, as well as a shape modification of L_2 edge absorption. The more realistic explanation lies in a different cation distribution. Fig. 2 shows the simulated absorption spectra for different Co^{2+} distributions between octahedral and tetrahedral sites, with

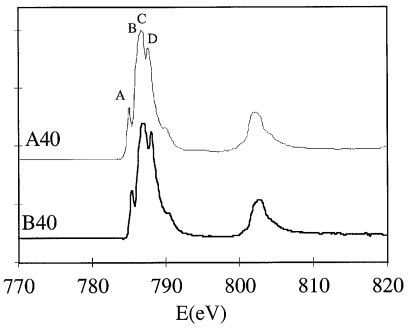

Fig. 1. Isotropic XAS spectra at 3 K at Co $L_{2,3}$ edges for samples A40 and B40.

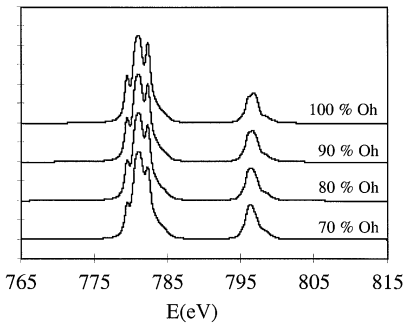

Fig. 2. Variation of theoretical isotropic XAS spectra at Co $L_{2,3}$ edges versus Co^{2+} site occupancy.

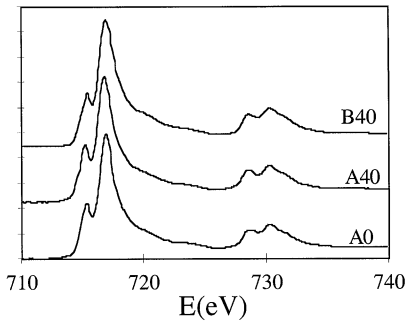

Fig. 3. Isotropic XAS spectra at 3 K at Fe $L_{2,3}$ edges for samples A0, A40 and B40.

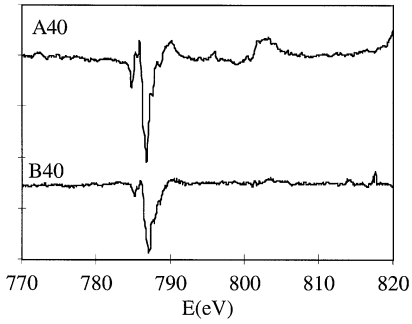

Fig. 5. XMCD spectra at 3 K at Co $L_{2,3}$ edges for samples A40 and B40.

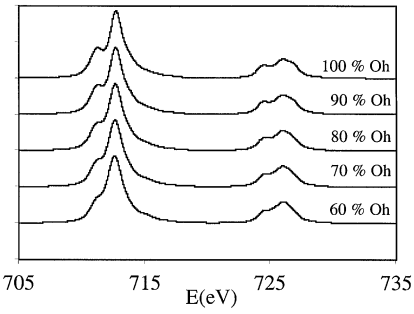

Fig. 4. Variation of theoretical isotropic XAS spectra at Fe $L_{2,3}$ edges versus Fe^{3+} site occupancy.

10 Dq = 1.2 eV (Oh) and 0.5 eV (Td), $\zeta_{3d} = 10$ meV and $\kappa = 70\%$. Occurrence of tetrahedral Co^{2+} induces the same spectra modifications as observed between B40 and A40, so Co^{2+} occupies only octahedral sites in B40 whereas a proportion around 20% of tetrahedral Co^{2+} is suggested in A40.

Neutron diffraction measurements performed on A0 sample indicates Zn^{2+} occupies tetrahedral sites with practically no inversion [19]. Hence since Co^{2+} occupies preferentially octahedral sites, we expect a different Fe^{3+} cationic distribution between A40 and A0 samples, with more tetrahedral Fe^{3+} in A40 than in A0. Fig. 3 shows the comparison between isotropic XAS spectra at Fe $L_{2,3}$ edges. The ratio of peak heights L_3/L_2 is slightly weaker (by a few percents) in A40 than in A0. The slight decrease of L_3/L_2 with increasing tetrahedral Fe^{3+} is evidenced by the simulation results shown in Fig. 4, with 10 Dq = 1.5 eV (Oh) and 0.7 eV (Td), $\kappa = 50\%$, but this effect is indeed very weak and insufficient to allow quantitative determinations. We can also remark that the obtained XAS spectra are sensitively different (at the two edges) from spectra of compounds containing Fe^{2+} [20–22].

Hence XAS spectra show Co^{2+} occupies octahedral sites in the smaller particles, whereas the distribution is more disordered in bigger particles. Octahedral preferential occupancy is not necessarily verified for Co^{2+} ions in ferrite nanoparticles obtained by soft chemistry. For example another group found that 10 nm particles of pure cobalt ferrite obtained by similar procedure were quite disordered, using neutron diffraction [23]. In our case the distribution is far from being random, due to the Zn^{2+} tetrahedral occupancy, making more difficult to obtain Co^{2+} in tetrahedral sites. Since the anisotropy of Co^{2+} is strong in octahedral sites and not in tetrahedral sites [24,25], the use of mixed cobalt–zinc ferrites is thought to be promising to increase the magnetocrystalline anisotropy of ferrite nanoparticles, even if compared to pure cobalt ferrite.

XMCD spectra at Co $L_{2,3}$ edges of samples A40 and B40 are very similar (Fig. 5), and it is difficult to show differences. In fact dichroism is weaker in sample B40 than in A40. The lower saturation magnetization results probably from increasing spin-canting when decreasing particle size. Simulated XMCD spectra show the ratio E3/E1 should decrease with increasing tetrahedral Co^{2+} content

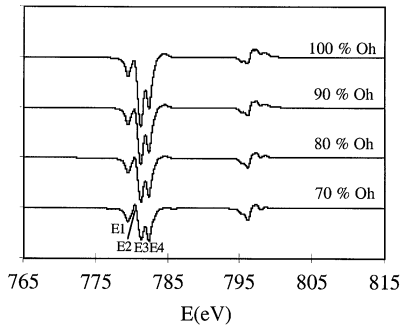

Fig. 6. Variation of theoretical XMCD spectra at Co $L_{2,3}$ edges versus Co^{2+} site occupancy.

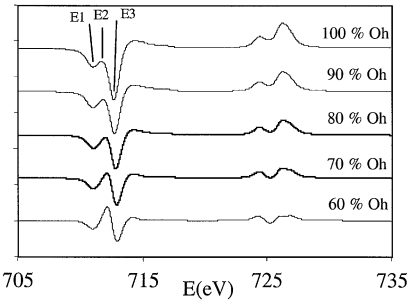

Fig. 8. Variation of theoretical XMCD spectra at Fe $L_{2,3}$ edges versus Fe^{3+} site occupancy.

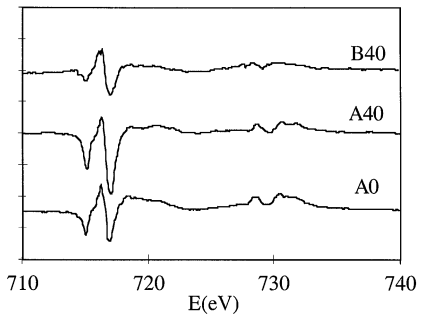

Fig. 7. XMCD spectra at 3 K at Fe $L_{2,3}$ edges for samples A0, A40 and B40.

(Fig. 6), but experimental spectra are not resolved enough to confirm this assumption. Moreover simulated XMCD spectra evidence that more sophisticated models are required to reproduce the experimental shape at L_3 edge.

Fig. 7 shows the XMCD signals for both samples A0 and A40 at Fe $L_{2,3}$ edges. The difference mainly lies in the ratio $E1/E3$. The simulated spectra with various cationic repartitions are shown on Fig. 8 The simulated ratio sensitively increases with tetrahedral occupancy, but the values obtained for this ratio are quite weak as compared to experimental data, hence a qualitative comparison is possible but not a quantitative determination of site repartition. Astonishingly, simulations suggest a higher proportion of tetrahedral Fe^{3+} in A0 than in A40, since this ratio varies from 0.6 in A40 to 0.8 in A0. This contradiction with the isotropic spectra in Fig. 3 comes from the underlying hypothesis of ferrimagnetic structure for A0. In the following we will consider a simple model inspired from Gilleo's approach [26]. Due to the strong dilution of tetrahedral sites by zinc ions, magnetic moments in octahedral sites are expected to be highly canted, which sensitively lowers the dichroic signal due to octahedral sites. If a magnetic ion in an octahedral site has no magnetic nearest neighbour in tetrahedral sites, it only interacts antiferromagnetically with the magnetic neighbours in octahedral sites. Its magnetic moment is then opposite to the general magnetic moments located in the octahedral sublattice. In the core of the nanoparticule the probability for a magnetic ion in octahedral site to be surrounded only by non-magnetic zinc ions in tetrahedral sites is $p_c\,(0)=x^6$, x being the fraction of tetrahedral sites occupied by zinc ions. At the surface the probability writes $p_s(0)=x^3$ with the hypothesis that half of the neighbours are lacking. When octahedral magnetic moments have only one magnetic neighbour in tetrahedral sites, the two antiferromagnetically coupled moments are also strongly canted to account for the intrasublattice antiferromagnetic couplings. In such a case $p_c\,(1)=6(1-x)x^5$ and $p_s(1)=3(1-x)x^2$. Table 1 shows the results for $p(0)$ and $p(\leqslant 1)=p(0)+p(1)$, considering $x=0.73$ (Zn^{2+} exclusively in tetrahedral sites) and $x=0.65$ (10% inversion for Zn^{2+} tetrahedral occupancy). Following this result a significant proportion of Fe^{3+} moments in octahedral sites is expected to be inverted or strongly canted. For the average size of 3.7 nm, 25% of the atoms are

Table 1
Probability for a magnetic moment in octahedral site to have zero ($p(0)$) or at maximum one ($p(\leqslant 1)$) magnetic neighbour in tetrahedral site, in the core or in the surface, with Zn^{2+} ions exclusively in tetrahedral sites ($x=0.73$) or with 10% inversion ($x=0.65$)

	$x=0.73$		$x=0.65$	
	Core	Surface	Core	Surface
$p(0)$	0.15	0.39	0.075	0.27
$p(\leqslant 1)$	0.49	0.82	0.32	0.72

located at the surface, hence from 13% ($x=0.65$) to 21% ($x=0.73$) Fe^{3+} moments in octahedral sites are inverted and at least 40% are canted. If 20% of the moments are inverted in octahedral sites, the total contribution of the octahedral sublattice is only 60% of its value if all the spins were parallel. This result is the example of the complementarity of the information extracted from isotropic and from XMCD spectra. Isotropic spectra are sensitive to the ratio between octahedral and tetrahedral site occupancy while XMCD signals are sensitive to the ratio of magnetic moments of the two sites.

Isotropic XAS allows an estimation of the cationic distribution of magnetic ions between tetrahedral and octahedral sites. XMCD is also sensitive to the magnetic structure. For small particles spin-canting may disturb the ferrimagnetic order, and because of the dilution of tetrahedral sites by nonmagnetic ions we expect strong canting angles or even inversion on the magnetic moments in octahedral sites

The evaluation of $\langle T_z\rangle$ from Ligand Field Multiplet calculation is about 1% of $\langle S_z\rangle$. So it can be neglected in the sum rules in first approximation. The B40 XMCD spectra exhibits practically no dichroism at L_2 edges, which means $\langle L_z\rangle$ is approximately as large as 4 $\langle S_z\rangle/3$. For A40 a more reliable integration of the peak area can be performed and leads to $\langle L_z\rangle=-\langle S_z\rangle$. The calculation results with $\zeta_{3d}=10$ meV leads to $\langle S_z\rangle=-1.26$ and $\langle L_z\rangle=-1.12$. This leads to a Co^{2+} magnetic moment of $3.64\,\mu_B$, which agrees with the expected magnetic moment per formula unit of pure cobalt ferrite [27]. To obtain the same values with the experimental data, the polarization rate must be evaluated around 40%, which is realistic. Another point is the calculation results for tetrahedral sites, leading to $\langle S_z\rangle=-1.50$ and $\langle L_z\rangle=-0.17$, evidencing the poor orbital moment of tetrahedral Co^{2+} ion as compared to octahedral one, which explains their difference in the contribution to magnetocrystalline anisotropy. It is noteworthy that the low ζ_{3d} value that was chosen for the simulation is also required to obtain values of $\langle L_z\rangle$ and $\langle S_z\rangle$ high enough [28–30]: if we calculate their values with $\zeta_{3d}=66$ meV (single ion calculation result) we obtain $\langle S_z\rangle=-1.00$ and $\langle L_z\rangle=-0.87$, which leads to magnetic moments weaker than $3\,\mu_B$, instead of the expected value around $3.7\,\mu_B$.

Hysteresis cycles are performed between -4 T and $+4$ T. Spectra at Fe $L_{2,3}$ edges are compared at various values of the field. The spectra recorded at 0 T after magnetization at $+4$ T and at 0 T after magnetization at -4 T give the remanent dichroism and can be compared to the saturation dichroism obtained at ± 4 T. This ratio of remanence over saturation (M_r/M_s) is obtained by using the intensities at 716.8 eV for L_3 Fe edge. As expected we observe a higher $M_r/M_s=0.40$ for the sample A40 containing cobalt ($y=0.40$) than for the sample A0 with $M_r/M_s=0.29$. This ratio is nevertheless approximately 30% weaker than expected from magnetization measurements. The discrepancy between XMCD results and magnetization curves could be due to the sample preparation, since for XMCD measurements we put a powder of particles into layers, leading to strong interactions between particles and drastic shape effects [31,32], whereas in SQUID experiments particles were dispersed in a polymer matrix. The same experiment could not be performed satisfactorily at Co $L_{2,3}$ edges because of the weaker dichroic signal due to the relative low cobalt content as compared to iron content.

Another characteristic point of hysteresis cycles is the coercive field. For the sample A40 we observe that absorption spectra at -0.2 T after magnetization at $+4$ T are identical to those at $+0.2$ T after magnetization at -4 T. Hence the coercive field is located at 0.2 T. For A0 sample, where no cobalt is present, the coercive field is too weak to repeat satisfactorily such investigation.

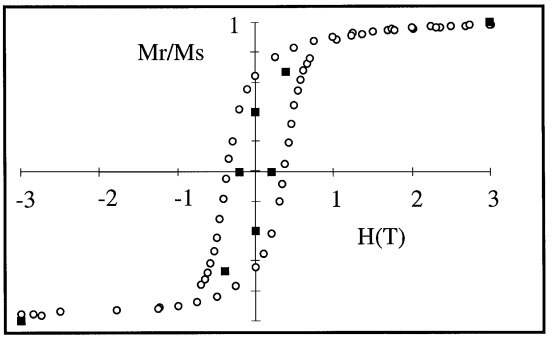

Fig. 9. Hysteresis curves at 3 K for sample A40: (○), SQUID measurements;(■), XMCD results at Fe^{3+} $L_{2,3}$ edges.

Hence hysteresis curves can be constructed thanks to XMCD measurements, as shown in Fig. 9. In our experiment some differences appear between XMCD and SQUID hysteresis cycles, nevertheless these discrepancies can be attributed to the samples preparation in both cases. For XMCD experiments nanoparticles are necessarily in a layer in powder form. Hence interactions between particles are expected to change significantly the hysteresis cycles, with a lower remanence than expected in the non-interacting case, since the applied field is perpendicular to the surface [33].

3. Conclusions

XAS and XMCD spectra allow an evaluation of the cationic distribution in mixed cobalt–zinc ferrite nanocrystals. Co^{2+} octahedral preferential occupancy is verified, which is not necessarily the case for nanocrystals obtained by soft chemistry and is partly attributed to the choice of a mixed composition with presence of tetrahedral Zn^{2+}. This method is therefore complementary to neutron diffraction, where refinement of the spectra is not easy for particles of a few nanometers, exhibiting substantial broadening of the diffraction lines and not necessarily well crystallized.

Hysteresis curves are performed thanks to XMCD measurements. This procedure uncouples the magnetic contributions of different magnetic ions and could be very promising for magnetic studies of mixed nanocrystals with enough magnetic ions content, for example in cases where the parallelism or antiparallelism between sublattices is generally disturbed by spin-canting, or in well defined core-shell nanoparticles. Hence this approach is a new tool to complete classical magnetometry measurements on complex systems, as also suggested by other recent experiments [34].

Acknowledgements

The authors thank J. Legrand, A.T. Ngo and N. Pinna (Laboratoire SRSI, Université Pierre et Marie Curie, Paris VI) for their assistance during the XMCD experiments. J.-P. Kappler is deeply thanked for his envolvement in the development of the cryogenic set-up. This is IPGP contribution number 1747.

References

[1] C.P. Bean, J.D. Livingston, J. Appl. Phys. 30 S (1959) 120S–129S.
[2] L. Néel, Ann. Geophys. 5 (1949) 99.
[3] J.M.D. Coey, Phys. Rev. Lett. 27 (1971) 1140.
[4] K. Haneda, A.H. Morrish, Phys. Lett. 64 A (1977) 259.
[5] B. Martinez, X. Obradors, L. Balcells, A. Rouanet, C. Monty, Phys. Rev. Lett. 80 (1998) 181.
[6] R.H. Kodama, A.E. Berkowitz, E.J. McNiff Jr., S. Foner, Mater. Sci. Forum 235–238 (1997) 643.
[7] R.H. Kodama, A.E. Berkowitz, Phys. Rev. B 59 (1999) 6321.
[8] A.E. Berkowitz, R.H. Kodama, S.A. Makhlouf, F.T. Parker, F.E. Spada, E.J. McNiff Jr., S. Foner, J. Magn. Magn. Mater. 196–197 (1999) 591.
[9] S. Sun, C.B. Murray, J. Appl. Phys. 85 (1999) 4325.
[10] S. Sun, C.B. Murray, J. Magn. Magn. Mater. 194 (1999).
[11] P.J. van der Zaag, A. Noordemer, M.T. Johnson, P.F. Bongers, Phys. Rev. Lett. 68 (1992) 3112.
[12] V.A.M. Brabers, Phys. Rev. Lett. 68 (1992) 3113.
[13] J.P. Chen, C.M. Sorensen, K.J. Klabunde, G.C. Hadjipanayis, E. Devlin, A. Kostikas, Phys. Rev. B 54 (1996) 9288.
[14] J.F. Hochepied, M.P. Pileni, J. Appl. Phys. 87 (2000) 2472.
[15] J.F. Hochepied, P. Bonville, M.P. Pileni, J. Phys. Chem. B 104 (2000) 905.
[16] C.F. Hague, J.-M. Mariot, G.Y. Guo, Phys. Rev. B 51 (1995) 1370.

[17] M.-A. Arrio, A. Scuiller, P. Sainctavit, C. Cartier dit Moulin, T. Mallah, M. Verdaguer, J. Am. Chem. Soc. 121 (1999) 6414.
[18] S. Imada, T. Jo, J. Magn. Magn. Mater. 104–107 (1992) 2001.
[19] J.-F. Hochepied, Thesis, Pierre et Marie Curie Paris VI, 1999.
[20] E. Pellegrin, M. Hagelstein, S. Doyle, H.O. Moser, J. Fuchs, D. Vollath, S. Schuppler, M.A. James, S.S. Saxena, L. Niesen, O. Rogojanu, G.A. Sawatzky, C. Ferrero, M. Borowski, O. Tjernberg, N.B. Brookes, Phys. Stat. Sol. B 215 (1999) 797.
[21] F. Schedin, P. Morrall, V.N. Petrov, S. Case, M.F. Thomas, E. Dudzik, G. van der Laan, G. Thornton, J. Magn. Magn. Mater. 211 (2000) 266.
[22] A. Mirone, M. Sacchi, S. Gota, Phys. Rev. B 61 (2000) 13540.
[23] A.J. Rondinone, A.C.S. Samia, Z.J. Zhang, J. Phys. Chem. B 103 (1999) 6876.
[24] P. Görnert, Phys. Stat. Sol. A 13 (1972) 101.
[25] M. Tachiki, Prog. Theoret. Phys. 23 (1960) 1055.
[26] M.A. Gilleo, J. Phys. Chem. Solids 13 (1960) 33.
[27] Landolt–Bornstein, Vol. 4b, 3rd Edition, Springer, Berlin, p. 385.
[28] C. Balhausen, Introduction to Ligand Field Theory, McGraw-Hill, New York, 1962.
[29] A.B.P. Lever, Inorganic Electronic Spectroscopy, 2nd Edition, Elsevier, Amsterdam, 1984.
[30] M.-A. Arrio, P. Sainctavit, C. Cartier dit Moulin, T. Mallah, M. Verdaguer, E. Pellegrin, C.T. Chen, J. Am. Chem. Soc. 118 (1996) 6422.
[31] D. Kechrakos, K.N. Trohidou, Phys. Rev. B 58 (1998) 12169.
[32] C.R. Pike, A.P. Roberts, K.L. Verosub, J. Appl. Phys. 88 (2000) 967.
[33] V. Russier, C. Petit, J. Legrand, M.P. Pileni, Phys. Rev. B 62 (2000) 3910.
[34] E. Goering, A. Fuss, W. Weber, J. Will, G. Schütz, J. Appl. Phys. 88 (2000) 5920.